n-Type Doping of Germanium from Phosphine: Early Stages Resolved at the Atomic Level

G. Scappucci,[1,*] O. Warschkow,[2] G. Capellini,[3] W. M. Klesse,[1] D. R. McKenzie,[2] and M. Y. Simmons[1]

[1]*School of Physics and Centre of Excellence for Quantum Computation and Communication Technology, University of New South Wales, Sydney, NSW 2052, Australia*

[2]*School of Physics and Centre of Excellence for Quantum Computation and Communication Technology, University of Sydney, Sydney, NSW 2006, Australia*

[3]*Dipartimento di Fisica "E. Amaldi," Università di Roma Tre, Via della Vasca Navale 84, 00146 Roma, Italy*

(Received 16 March 2012; published 13 August 2012)

To understand the atomistic doping process of phosphorus in germanium, we present a combined scanning tunneling microscopy, temperature programed desorption, and density functional theory study of the reactions of phosphine with the Ge(001) surface. Combining experimental and theoretical results, we demonstrate that $PH_2 + H$ with a footprint of one Ge dimer is the only product of room temperature chemisorption. Further dissociation requires thermal activation. At saturation coverage, $PH_2 + H$ species self-assemble into ordered patterns leading to phosphorus coverages of up to 0.5 monolayers.

DOI: 10.1103/PhysRevLett.109.076101 PACS numbers: 68.35.−p, 68.37.Ef, 68.47.Fg, 73.20.Hb

n-type doping of germanium at high concentrations is currently the subject of intense research, because it lies at the heart of seminal developments such as ultrashallow junctions for next generation high-speed transistors [1], complementary metal-oxide-semiconductor–compatible integrated lasers [2], and Ge devices fabricated at the atomic scale [3]. *In situ* doping techniques are of particular interest because of their compatibility with conventional fabrication processes and their potential to achieve high doping levels while avoiding the damage associated with ion implantation techniques [4]. We have recently demonstrated an atomic-layer doping process using phosphine (PH_3) gas to achieve atomically sharp phosphorus dopant profiles in germanium at high planar concentrations ($\sim 10^{14}$ cm^{-2}) [5]. These experimental studies established the viability of this *in situ* doping technique by addressing several critical material science challenges, namely, obtaining a near-defect-free Ge(001) surface [6] and determining the optimal growth parameters to achieve high crystal quality while maintaining vertical dopant confinement [7]. Importantly, this doping technique has been combined with scanning-probe lithography to demonstrate lateral dopant confinement [3] and, thus, a complete fabrication route for three-dimensionally patterned, atomic-scale, donor-based devices in Ge. With this Letter, we present a combined experimental and theoretical study into the chemisorption of PH_3 molecules on the Ge(001) surface, a critical step of the atomic-layer doping process. Using scanning tunneling microscopy (STM), temperature programed desorption (TPD), and density functional theory, we identify the key adsorbate species formed and resolve the early stages of the doping process at an atomic level.

Scanning tunneling microscopy experiments were performed at room temperature in an Omicron ultrahigh vacuum system (base pressure $<5 \times 10^{-11}$ mbar) with separate chambers for PH_3 dosing, STM imaging, and Ge deposition. Germanium (001) samples 2.5×10 mm^2 in size were cleaved from a Sb-doped wafer. Atomically flat and defect-free surfaces were prepared by using a combination of *ex situ* wet etch, *in situ* thermal anneal, and Ge molecular beam epitaxy (see Ref. [6] for details).

Figures 1(a) and 1(b) show filled-state STM images of the Ge(001) before and after exposure to a low dose (7.5×10^{-4} L) of phosphine at room temperature. Both images exhibit the characteristic [8] $p(2 \times 1)$ and $c(4 \times 2)$ reconstruction domains of Ge(001). Two distinct new features appear in the postexposure image due to PH_3 chemisorption [boxes in Fig. 1(b)]. Both features are one dimer wide with an asymmetric appearance: a bright protrusion that is offset from the center of the dimer row and a dark depression at the opposite dimer end. However, their appearance is different depending on their $p(2 \times 1)$ or $c(4 \times 2)$ environment (bright and dim boxes, respectively). Figure 1(c) shows STM line profiles along two ends of the same dimer row. These profiles illustrate that the apparent height difference between protrusions and corresponding depressions is ~170 pm on $p(2 \times 1)$ and ~70 pm on $c(4 \times 2)$; thus, the former appear with higher contrast. Yet, the apparent height of the protrusions against the dimer row average is comparable (approximately 99 and 85 pm, respectively) suggesting that these features correspond to the same chemical species. This is confirmed by close-up images [Figs. 1(d) and 1(e)] recorded in dual bias mode ($\pm$ 1.3 V): For both types of features, the bright protrusion occurs on the same dimer end in filled and empty states. This observation suggests that the asymmetric features are $PH_2 + H$ [Fig. 1(f)], by analogy to the well-studied PH_3/Si(001) system [9,10] where $PH_2 + H$ adsorbates have a strikingly similar appearance (see Figs. 1 and 4 in Ref. [9]). Crucially, on Ge(001) we do not observe the prominent dimer-centered feature that corresponds to $PH + 2H$ on Si(001). Thus, our STM-based analysis

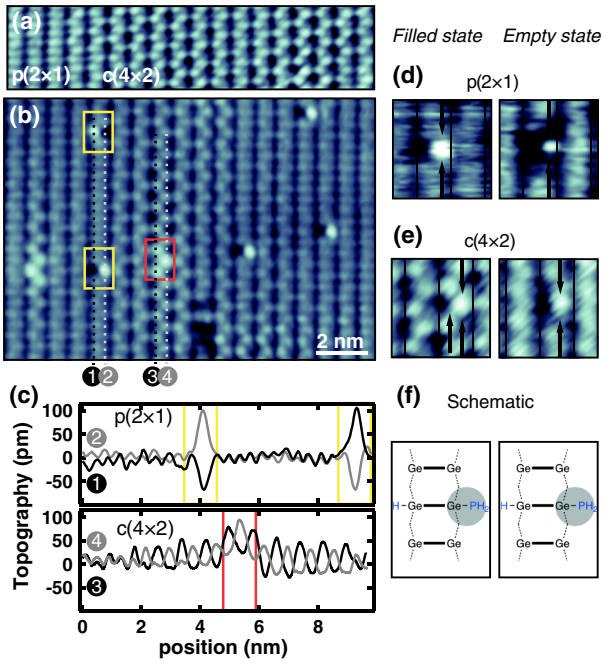

FIG. 1 (color online). (a) Filled-state STM image of the clean Ge(001) surface, with domains of $p(2 \times 1)$ and $c(4 \times 2)$ reconstructions. (b) The surface after low-coverage dosing with PH_3 showing asymmetric features on both $p(2 \times 1)$ and $c(4 \times 2)$ reconstructions (bright and dim boxes, respectively). (c) Line profiles across along two ends of the same dimer row. (d), (e) Filled- and empty-state close-up images of the asymmetric features as they appear on $p(2 \times 1)$ and $c(4 \times 2)$, respectively. (f) Schematic indicating the imaging sites of on-dimer $PH_2 + H$ in filled and empty state by analogy to $PH_2 + H$ on Si(001) (see the text).

suggests a major difference in how PH_3 reacts at room temperature with Ge(001) and Si(001), despite the intuitive similarity between these two surfaces [8].

In order to further understand this reaction, we performed density functional theory calculations using the GAUSSIAN 09 software [11] and a computational approach that we refer to as a *compound cluster model* [12]. The calculation of accurate adsorption energies requires a high-level treatment of exchange-correlation, a large cluster, and a large basis set [13], which tends to be impractically expensive in a single, all-in-one calculation. Instead, the compound cluster model combines the results of several computations into a single energy expression. A first approximation to the adsorption energy is calculated by using a small two-dimer $Ge_{15}H_{16}$ cluster representation of the Ge(001) surface, a high-quality hybrid exchange-correlation functional (HSE06; Ref. [14]), and a large composite type basis set [15]. This energy is then corrected for cluster size [12,13] by using a larger four-dimer $Ge_{53}H_{44}$ cluster and the more economic generalized gradient approximation to density functional theory. This correction accounts for the strain effect of at least one free, buckled dimer on either side of the adsorbate. All atoms are fully relaxed in our calculations except for the cluster-terminating hydrogen atoms, which are held fixed. Full details of the computational procedure can be found in Ref. [12]. For additional examples of the ability of this method to describe chemical processes observed in STM, see Refs. [16,17].

The calculated reaction path and energy profile of PH_3 on Ge(001) are outlined in Figs. 2(a) and 2(b), respectively. The intermediate structures that occur in this figure break down into three groups according to the degree of nominal PH_3 fragmentation: molecularly adsorbed PH_3 (one configuration, structure $A1$), $PH_2 + H$ (four configurations, $B1$ to $B4$), and $PH + 2H$ (two configurations, $C1$ and $C2$). As illustrated in Fig. 2(a), these configurations interconvert into one another by a combination of dissociative H-shift reactions and PH_x diffusion reactions. Considering the energies of the most stable configuration within each group, namely, structures $A1$ (-0.79 eV), $B1$ (-1.59 eV), and $C1$ (-2.05 eV), we see that each step of PH_3 dissociation results in a substantial gain in thermodynamic stability.

Room temperature chemisorption reactions on semiconductors are typically governed by kinetics. Highlighted in Fig. 2(b) (red arrows) are three activation energies, E_A, that are critical to our experimental observations. The first barrier (0.54 eV) determines the rate of dissociation of the molecular PH_3 adsorbate $A1$ into a $PH_2 + H$ structure. Of the two possibilities considered ($A1 \rightarrow B1$ and $A1 \rightarrow B2$), the interdimer H-shift reaction producing structure $B2$ is kinetically preferred with an activation energy of 0.54 eV. Via the Vineyard equation [18], we calculate an attempt frequency of 2.2×10^{12} s^{-1} for this process, which leads for structure $A1$ to an estimated room temperature lifetime (or inverse Arrhenius rate) of $\tau_{A1} = 6 \times 10^{-4}$ s. This result firmly rules out molecularly adsorbed PH_3 as an observable species in our STM experiments (imaging time scale of minutes to hours). The second highlighted barrier of 0.41 eV governs the rearrangement of the interdimer structure $PH_2 + H$ ($B2$) into the thermodynamically more favorable on-dimer configuration $B1$. This reaction is also calculated to be fast (lifetime $\tau_{B2} = 1 \times 10^{-6}$ s) under experimental time scales, which explains the absence of any two-dimer wide $PH_2 + H$ features in our image data. Last, the dissociation of on-dimer $PH_2 + H$ into the much more stable $PH + 2H$ structure $C1$ is controlled by the third highlighted activation energy (1.19 eV) in Fig. 2(b). Again, we considered two plausible routes for this reaction ($B1 \rightarrow B3 \rightarrow B4 \rightarrow C1$ and $B1 \rightarrow B3 \rightarrow C2 \rightarrow C1$). Both routes have the same net activation energy of 1.19 eV; however, the path via $B3$ and $C2$ is slightly preferred due to a larger attempt frequency. Either way, the on-dimer $PH_2 + H$ species is predicted to be stable at room temperature ($\tau_{B1} > 10^9$ s) and dissociation into $PH + 2H$ does not occur. These theoretical results unambiguously confirm the observed STM features in our images [Fig. 1(b)] as on-dimer $PH_2 + H$, and they explain the absence of any other stable adsorbate configurations, including $PH + 2H$. Only

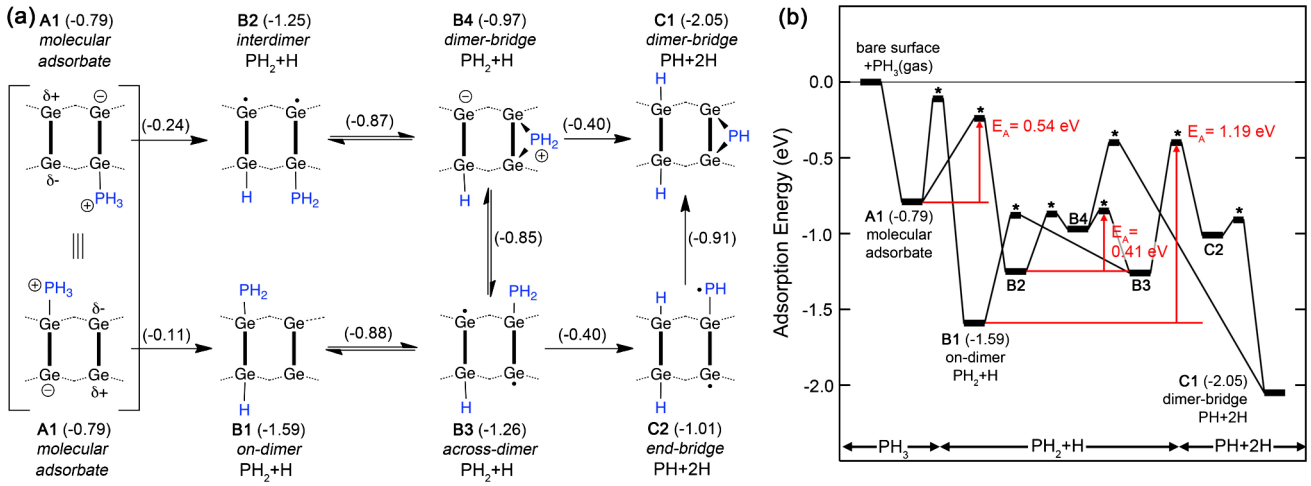

FIG. 2 (color online). (a) Schematic valence structure outline of PH_3 dissociation of Ge(001). Thick vertical bars indicate the Ge-Ge dimers of the surface. Intermediate structures and reaction arrows (i.e., transition states) are annotated with the calculated energy (in eV). (b) Schematic potential energy profile with transition state structures labeled with a "$*$" character. Three activation energies critical to PH_3/Ge(001) chemisorption are indicated with red arrows. All energies are given in eV.

at higher temperatures can we expect $PH_2 + H$ to dissociate at an appreciable rate (e.g., $\tau_{B1} = 36$ s at 150 °C).

Moving on from low-coverage dosing and isolated adsorbates, we now investigate the Ge(001) surface dosed to saturation at room temperature. An earlier x-ray photoemission spectroscopy study by Tsai and Lin [19] concluded that molecularly adsorbed PH_3 is the primary product formed under these high-coverage conditions. Figure 3(a) shows a filled-state STM image of Ge(001) exposed to 2.3 L of PH_3 with a prominent step edge running diagonally across the image. Within the terraces, the $p(2 \times 1)$ and $c(4 \times 2)$ dimer patterns of clean Ge(001) are no longer apparent; instead, a dense distribution of protrusions is seen that exhibits a degree of local order into *linear* or *zigzag* patterns [see boxes (1) and (2) in Fig. 3(a), respectively]. Several clues suggest that these protrusion patterns arise not from molecularly adsorbed PH_3 but from a dense packing of $PH_2 + H$ species as illustrated in Fig. 3(b). This is confirmed by counting statistics over several images (total area of $\sim$10 000 nm^2), which reveals a protrusion density of 0.46 ± 0.05 ML. This is almost one dissociated PH_3 for every Ge-Ge dimer and can be best explained by a $PH_2 + H$ dissociate. Additionally, the pairing of protrusions and depressions on a single dimer is similar to that observed for the isolated $PH_2 + H$ species in our low-coverage data. Finally, strikingly similar linear and zigzag patterns have been reported earlier for the analogous NH_3/Si(001) chemisorption system [20], where they have been attributed to ordered $NH_2 + H$ adsorbates. Collectively, these results confirm that again $PH_2 + H$ is the only species formed in our high-coverage experiments. This too is different from Si(001), for which a saturation dose produces both $PH_2 + H$ and $PH + 2H$ [10].

Importantly, these findings suggest that the PH_3/Ge(001) system is less akin to PH_3/Si(001) than intuition would suggest. In fact, key aspects of the chemisorption process more closely resemble the NH_3/Si(001) system. With hindsight, this trend can be made plausible by considering P-Ge and N-Si bond lengths (2.45 and 1.7 Å, respectively), which are shorter than the corresponding Ge-Ge and Si-Si bonds (2.49 and 2.33 Å, respectively). These shorter bond lengths result in higher barriers, thus requiring higher temperatures to effect dissociation. In contrast, the P-Si bond (2.36 Å) is longer than the Si-Si bond (2.33 Å) facilitating $PH_2 + H$ diffusion and dissociation on Si(001).

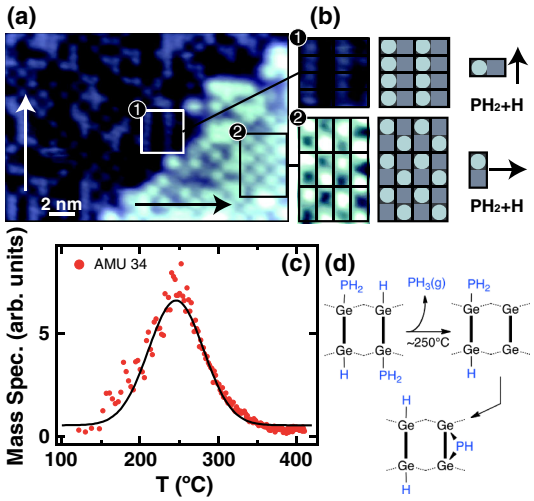

FIG. 3 (color online). (a) Filled-state STM image of a Ge(001) surface saturation dosed with PH_3 at room temperature, along with (b) close-up images and schematics of linear and zigzag coadsorption patterns of $PH_2 + H$ species. The dimer row directions are indicated for clarity with arrows. (c) TPD spectrum of a saturated-dosed Ge(001) surface with a mass 34 amu single peak attributed to the recombinative desorption or dissociation of $PH_2 + H$ as illustrated in (d).

Further insights into the thermal properties of a PH_3 saturation-dose Ge(001) surface are gained from mass-resolved TPD experiments. Samples were direct-current heated at a controlled rate of 1 K/s in line of sight of a quadrupole mass spectrometer (Pfeiffer). Figure 3(c) shows the TPD spectrum for detected mass 34 amu (PH_3) which exhibits a single peak centered at $250 \pm 5\,^{\circ}C$ due to the desorption of PH_3 from the Ge surface. By using the Redhead peak-maximum equation [21], we obtain an activation energy of 1.48 ± 0.12 eV, with an assumed attempt frequency in the range 10^{12}–$10^{14} s^{-1}$. We assign this PH_3 desorption process to $PH_2 + H$ recombination for which our low-coverage energetics diagram [Fig. 2(b); structure $B1$] suggests an activation energy of 1.59 eV in good agreement with the experimental value. Note here that the preferred dissociation into PH + 2H is initially suppressed, because the free dimers required are absent at high coverage. However, every recombinative thermal desorption step creates a single free dimer as outlined in Fig. 3(d), allowing another $PH_2 + H$ species to dissociate into PH + 2H. Thus, at high coverage, the rate of $PH_2 + H$ dissociation is determined by the barrier of PH_3 desorption (calculated 1.59 eV) and not the dissociation barrier itself (i.e., 1.19 eV). This interpretation neatly connects with the earlier x-ray photoemission spectroscopy measurements by Tsai and Lin [19] if we assume that the observed P-2p components are PH_2, PH, and P (not PH_3, PH_2, and P as reported in Ref. [19]). Starting with a single P-2p component in their x-ray photoemission spectroscopy data [Fig. 1(a) in Ref. [19]] at room temperature, the emergence of a second component occurs at a temperature range of 200–300 °C. This matches our 250 °C TPD peak and is thus consistent with the onset of the $PH_2 + H$ to PH + 2H reaction [Fig. 3(d)].

In summary, our experimental data and theoretical modeling unambiguously determine $PH_2 + H$ as the only product of room temperature PH_3 chemisorption on Ge(001). This applies to both low and saturation coverages, leading to a maximal phosphorus coverage of 0.5 ML (i.e., a planar dopant density of 3×10^{14} cm^{-2}). The recombinative PH_3 desorption process revealed in our TPD experiments suggests that thermal anneals at 250 °C and above are likely to reduce the P coverage by up to 50%. A notable feature of PH_3/Ge(001) is the counterintuitive similarity with NH_3/Si(001), rather than PH_3/Si(001), which we can understand in terms of bond length ratios. These atomic-scale insights provide crucial information to optimize the thermal annealing protocols of the atomic-layer deposition process. Moreover, these results have important implications in the emerging field of solitary dopant optoelectronics (or solotronics; Ref. [22]), for which the formation of only a single species $PH_2 + H$ upon phosphine chemisorption is bound to simplify the development of a robust process to fabricate Ge-based solotronic devices with deterministic P dopant placement.

This work was supported by the Australian Research Council through the Centre of Excellence for Quantum Computation and Communication Technology (Project No. CE1100096). G. S. and G. C. acknowledge support from UNSW (2011 Science Faculty Research Grant). M. Y. S. acknowledges an Australian Government Federation Fellowship. Computational resources used in this work were provided by the Australian National Computational Infrastructure.

*giordano.scappucci@unsw.edu.au

[1] R. Pillarisetty, Nature (London) **479**, 324 (2011).
[2] D. Liang and J. E. Bowers, Nature Photon. **4**, 511 (2010).
[3] G. Scappucci, G. Capellini, B. Johnston, W. M. Klesse, J. A. Miwa, and M. Y. Simmons, Nano Lett. **11**, 2272 (2011).
[4] G. D. Dilliway *et al.*, ECS Trans. **3**, 599 (2006).
[5] G. Scappucci, G. Capellini, W. M. Klesse, and M. Y. Simmons, Nanotechnology **22**, 375203 (2011).
[6] W. M. Klesse, G. Scappucci, G. Capellini, and M. Y. Simmons, Nanotechnology **22**, 145604 (2011).
[7] G. Scappucci, G. Capellini, and M. Y. Simmons, Phys. Rev. B **80**, 233202 (2009).
[8] H. J. W. Zandvliet, Phys. Rep. **388**, 1 (2003).
[9] H. F. Wilson, O. Warschkow, N. A. Marks, S. R. Schofield, N. J. Curson, P. V. Smith, M. W. Radny, D. R. McKenzie, and M. Y. Simmons, Phys. Rev. Lett. **93**, 226102 (2004).
[10] S. R. Schofield, N. J. Curson, O. Warschkow, N. A. Marks, H. F. Wilson, M. Y. Simmons, P. V. Smith, M. W. Radny, D. R. McKenzie, and R. G. Clark, J. Phys. Chem. B **110**, 3173 (2006).
[11] M. J. Frisch *et al.*, GAUSSIAN 09, v. Revision C.01, Wallingford CT, Gaussian, Inc., 2009.
[12] O. Warschkow, I. Gao, S. R. Schofield, D. R. Belcher, M. W. Radny, S. A. Saraireh, and P. V. Smith, Phys. Chem. Chem. Phys. **11**, 2747 (2009).
[13] O. Warschkow, T. L. McDonell, and N. A. Marks, Surf. Sci. **601**, 3020 (2007).
[14] J. Heyd, G. E. Scuseria, and M. Ernzerhof, J. Chem. Phys. **118**, 8207 (2003); **124**, 219906 (2006).
[15] Single-point energy calculations were conducted by using a standard 6-311G(2df,2pd) basis set with additional ++ diffuse functions on the adsorbate and dimer atoms. Geometry optimizations utilize a more compact basis set labeled BS1, which is defined in Ref. [13].
[16] O. Warschkow, D. R. Belcher, M. W. Radny, S. R. Schofield, and P. V. Smith, Phys. Rev. B **84**, 153302 (2011).
[17] O. Warschkow, S. R. Schofield, N. A. Marks, M. W. Radny, P. V. Smith, and D. R. McKenzie, Phys. Rev. B **77**, 201305(R) (2008).
[18] G. H. Vineyard, J. Phys. Chem. Solids **3**, 121 (1957).
[19] H. W. Tsai and D. S. Lin, Surf. Sci. **482**, 654 (2001).
[20] D. R. Bowler and J. H. G. Owen, Phys. Rev. B **75**, 155310 (2007).
[21] P. A. Redhead, Vacuum **12**, 203 (1962).
[22] P. M. Koenraad and M. E. Flatte, Nature Mater. **10**, 91 (2011).